

1 **Photoenhanced sulfates formation by the heterogeneous uptake of SO₂ on non-**
2 **photoactive mineral dust**

3 Wangjin Yang, Jiawei Ma, Hongxing Yang, Fu Li, Chong Han*

4 School of Metallurgy, Northeastern University, Shenyang, 110819, China

5 *Address correspondence to author: hanch@smm.neu.edu.cn

6

7 **Short summary.** We provide direct evidences that light prominently enhances the conversion
8 of SO₂ to sulfates on non-photoactive mineral dust, where triplet states of SO₂ (³SO₂) can act
9 as a pivotal trigger to generate sulfates. Photochemical sulfate formation depends on H₂O, O₂,
10 and basicity of mineral dust. It is suggested that the SO₂ photochemistry on non-photoactive
11 mineral dust significantly contributes to sulfates, highlighting previously unknown pathway to
12 better explain the missing sources of atmospheric sulfates.

13

14 **Abstract.** Heterogeneous uptake of SO₂ on mineral dust is a predominant formation pathway
15 of sulfates, whereas the contribution of photo-induced SO₂ oxidation to sulfates on the dust
16 interfaces still remains unclear. Here, we investigated heterogeneous photochemical reactions
17 of SO₂ on five mineral oxides (SiO₂, kaolinite, Al₂O₃, MgO, and CaO) without photocatalytic
18 activity. Light significantly enhanced the uptake of SO₂, and its enhancement effects negatively
19 depended on the basicity of mineral oxides. The initial uptake coefficient ($\gamma_{0, \text{BET}}$) and the
20 steady-state uptake coefficient ($\gamma_{s, \text{BET}}$) of SO₂ positively relied on light intensity, relative
21 humidity (RH) and O₂ content, while they exhibited a negative relationship with the initial SO₂
22 concentration. Rapid sulfate formation during photo-induced heterogeneous reactions of SO₂
23 with all mineral oxides was confirmed to be ubiquitous, and H₂O and O₂ played the key roles
24 in the conversion of SO₂ to sulfates. Specially, triplet states of SO₂ (³SO₂) was suggested to be
25 the trigger for photochemical sulfate formation. Atmospheric implications supported a
26 potential contribution of interfacial SO₂ photochemistry on non-photoactive mineral dust to
27 atmospheric sulfate sources.

28

29 **Keywords:** SO₂; Sulfates; Non-photoactive mineral dust; Heterogeneous photochemistry

30

31

32 **1 Introduction**

33 As an important trace gas in the atmosphere, SO₂ is mainly emitted by volcanic eruption and
34 fuel combustion. There is an uneven distribution of atmospheric SO₂ concentrations that show
35 a distinctive seasonal and regional differentiation. Typical ratios of SO₂ in the troposphere are
36 below 0.5 ppb for a clean weather in remote areas, rising to around several hundred ppb during
37 the polluted days in urban regions (Ma et al., 2020). About half of SO₂ is oxidized to sulfates
38 (He et al., 2012), which is one of the most significant compositions in fine particles. The mass
39 fraction of sulfates in PM_{2.5} is high up to 30% (Shao et al., 2019), especially in polluted regions
40 where high-sulfur fuels are usually used (Olson et al., 2021). They significantly alter
41 physicochemical properties of aerosols in terms of hygroscopicity, acidity and light absorption
42 property (Chan and Chan, 2003; Cao et al., 2013; Lim et al., 2018). Sulfates also pose a human
43 health risk through causing respiratory illness and cardiovascular (Shiraiwa et al., 2017). In
44 addition, the deposition of sulfates leads to adverse effects on ecosystems via the acidification
45 of soils and lakes (Golobokova et al., 2020). Therefore, the oxidation of SO₂ to form sulfates
46 has attracted widespread attention in the past decades.

47 The conversion of SO₂ to sulfates in the atmosphere usually occurs in different phases: gas-
48 phase oxidation of SO₂ by hydroxyl radicals (\bullet OH) or Criegee intermediate radicals (Mauldin
49 et al., 2012; Davis et al., 1979); aqueous-phase reaction of SO₂ with O₃, peroxides or transition
50 metal ions dissolved in cloud and fog droplets (Alexander et al., 2009; Herrmann et al., 2000;
51 Harris et al., 2013; Liu et al., 2020a; Li et al., 2020); and heterogeneous SO₂ uptake on aerosols
52 including authentic mineral dust, soot, inorganic ion and organic compounds (Adams et al.,
53 2005; He et al., 2018a; Ye et al., 2018; Wang et al., 2019; Yao et al., 2019; Zhang et al., 2020a;
54 Liu et al., 2020; Liu et al., 2021). However, the oxidation of SO₂ in gas and aqueous phases
55 fails to explain high sulfate concentrations under polluted conditions. Model simulation

56 suggests that the rapid sulfate formation can be attributed to the heterogeneous SO₂ uptake (Li
57 et al., 2017). A positive relationship between the fraction of sulfates and mineral dust in haze
58 days has been reported, implying that mineral dust may account for the formation of sulfates
59 (Wang et al., 2020a). Moreover, a large amount of sulfates was observed to be formed on the
60 surface of mineral dust after long-distance transport (Prospero, 1999). Thus, investigating the
61 heterogeneous oxidation of SO₂ on mineral dust can provide basic data for the model
62 calculation to evaluate atmospheric sulfates.

63 Mineral dust, regarded as the dominant component of particulate matters in the atmosphere,
64 accounts for about 30%–60% mass fractions of global aerosols (Dentener et al., 1996; Peng et
65 al., 2012). It primarily contains SiO₂ (40%–80%), followed by Al₂O₃ (10%–15%), Fe₂O₃
66 (6%–13%), CaO (3%–10%), MgO (1%–7%) and TiO₂ (0.1%–5%) (Urupina et al., 2021;
67 Urupina et al., 2019; Usher et al., 2003). Mineral dust can provide active sites for adsorption
68 and reaction of gases. Up to now, the heterogeneous SO₂ uptake on authentic mineral aerosols
69 and model mineral oxides has been widely reported (Ma et al., 2019; Goodman et al., 2001;
70 Wang et al., 2018; Wang et al., 2020b), with various uptake coefficients (γ) of SO₂ varying
71 from 10⁻⁹ to 10⁻⁴ (Urupina et al., 2019; Usher et al., 2002).

72 It was recognized that light could significantly enhance heterogeneous conversion of SO₂ to
73 sulfates on the surface of photocatalytic mineral dust (Chen et al., 2021; Li et al., 2019; Wang
74 et al., 2020b). Electron-hole pairs are produced via photo-induced electrons from the valence
75 band to the conduction band of photocatalytic metal oxides, and then react with H₂O and O₂ to
76 generate reactive oxygen species (ROS), such as •OH and •O₂⁻ (Chu et al., 2019). Sulfates are
77 produced by the heterogeneous reactions of SO₂ with ROS (Park and Jang, 2016; Park et al.,
78 2017; Langhammer et al., 2020; Bounechada et al., 2017). In particular, due to the large
79 abundance of non-photoactive mineral dust (more than 85% mass of total mineral dust in the
80 atmosphere) (Usher et al., 2003; Liu et al., 2022), revealing the photooxidation processes of
81 SO₂ on these mineral dust is of great importance to better reevaluate the sulfate formation on
82 aerosols in the global scale.

83 Hence, photochemical SO₂ uptake and sulfate formation on non-photoactive mineral oxides

84 were firstly investigated using a flow reactor and an *in situ* diffuse reflectance infrared Fourier
85 transform spectroscopy (DRIFTS). The SO₂ conversion to sulfates was examined under various
86 conditions, and the roles of light intensity, SO₂ concentration, H₂O, O₂ and basicity of mineral
87 oxides were determined. Reaction mechanisms and atmospheric implications were proposed,
88 highlighting a new and important pathway accounting for photochemical uptake of SO₂ to form
89 sulfates on the non-photoactive surfaces.

90

91 **2 Experimental methods**

92 **2.1 Materials**

93 Analytical grade SiO₂ (Sinopharm Chemical Reagent Co., Ltd.), kaolinite (Sinopharm
94 Chemical Reagent Co., Ltd.), Al₂O₃ (Alfa Aesar), MgO (Sigma-Aldrich), and CaO (Sigma-
95 Aldrich) were used in the experiments. Through the nitrogen Brunauer-Emmett-Teller (BET)
96 physisorption analysis, their specific surface areas were detected to be 0.419, 6.407, 8.137,
97 10.948 and 6.944 m² g⁻¹, respectively. With BaSO₄ used as the reference, the ultraviolet-visible
98 (UV-vis) light absorption spectra of samples (Figure S1) in the wavelength range of 300–800
99 nm were obtained by the Shimadzu UV-2550 spectrophotometer, which was equipped with
100 diffuse reflection integrating sphere attachment. The solid powder (0.2–5 g) was uniformly
101 dispersed into 10.0 mL ethanol solution. The mixed liquid was poured into a rectangle quartz
102 sample dish (14.0 cm × 7.0 cm) and dried to form a solid coating in an oven at 353 K for 10 h.
103 SO₂ standard gas (50 ppm in N₂, Shenyang Air Liquide Co., LTD) and high purity N₂ and O₂
104 (99.999 vol.%, Shenyang Air Liquide Co., LTD) were used as received. The solid sample
105 powder (0.2 g) was immersed into 10 mL deionized water (20 mg mL⁻¹), and then the
106 suspension was vigorously stirred for 10 min. The pH of SiO₂, kaolinite, Al₂O₃, MgO and CaO
107 suspension was measured to be 6.27, 6.58, 9.33, 10.61 and 12.72 using a pH meter, respectively,
108 which was employed to characterize the basicity of mineral oxides.

109 **2.2 Rectangular flow reactor**

110 The uptake experiments of SO₂ on mineral dust were performed in a horizontal rectangular
111 flow reactor (26.0 cm length × 7.5 cm width × 2.0 cm height), which was depicted in Figure

112 S2. In a previous study, a similar rectangular flow reactor was designed and the feasibility of
113 the reactor has been verified (Knopf et al., 2007). The reactor was made of quartz to allow the
114 transmission of light. The temperature was maintained at 298 K by circulating temperature-
115 controlled water through the outer jacket of the reactor. Synthetic air with a N₂/O₂ volume ratio
116 of 4:1 was introduced into the flow reactor, and its total flow rate was 1000 mL min⁻¹. The
117 Reynolds number (*Re*) was calculated to be 28.2 (*Re* < 200), as described in the Supporting
118 Information, indicating a laminar flow state. SO₂ with high purity N₂ (100 mL min⁻¹) as carrier
119 gas were introduced into the reactor through a movable T-shaped injector equipped with six
120 exit holes of 0.2 mm diameter, so that the gas could be uniformly distributed over the width of
121 the reactor. The SO₂ concentration was 40–200 ppb and measured with a SO₂ analyzer (Thermo
122 43i). Wet N₂ generated with a bubbler containing deionized water was introduced by two
123 parallel inlets on the side of T-shaped injector. Relative humidity (RH, 10%–75%) was
124 controlled by regulating the ratio of dry N₂ to wet N₂ and measured via a hygrometer (Center
125 314). The equivalent layer numbers of water on surface was 0.9–4.0 according to the Brunauer-
126 Emmett-Teller (BET) model (Sumner et al., 2004), and the thickness of the film of adsorbed
127 water varied between 2.7–12 nm at RH=10%–75%. There were three equally spaced exhaust
128 ports to mitigate the outlet turbulence. A xenon lamp (CEL-LAX500, China Education Au-light
129 Co., Ltd) was used to simulate sunlight and vertically located above the reactor. A filter was
130 placed on the reactor to remove the light with wavelengths shorter than 300 nm. The spectrum
131 irradiance of the xenon lamp was displayed in Figure S3 and measured using a calibrated
132 spectroradiometer (ULS2048CL-EVO, Avantes). The spectral irradiance was measured inside
133 the reactor, after passing the water cooling and in the absence of a sample. The total irradiance
134 ($0-7.93 \times 10^{16}$ photons cm⁻² s⁻¹) on the coating can be adjusted by varying the distance of the
135 xenon lamp to the reactor.

136 **2.3 Uptake coefficient of SO₂**

137 The heterogeneous reaction kinetics of SO₂ with mineral dust can be described by a pseudo-
138 first-order reaction. SiO₂ was taken as an example, and Figure S4 showed a linear relationship
139 between the natural logarithm of the SO₂ concentration and the reaction time. The apparent rate

140 constant ($k_{\text{obs, SiO}_2}$) of SO₂ with SiO₂ can be calculated using the equation 1,

141
$$\frac{\ln(C_0/C_t)}{t} = k_{\text{obs, SiO}_2} \quad (1)$$

142 where C_0 and C_t (ppb) are the initial SO₂ concentration and the SO₂ concentration, respectively;
143 t was calculated by dividing the length of the reactive surface by the average flow velocity. The
144 loss of SO₂ on the internal wall of the reactor in blank experiments was carried out under
145 various conditions (Figure S5 as an example), and it has been deducted for the γ calculation.
146 Assuming that the wall loss was constant in the experiments with and without samples, the
147 geometric uptake coefficient (γ_{geo}) was determined by the equation 2 (Knopf et al., 2007),

148
$$\gamma_{\text{geo}} = \frac{4Vk}{S\omega} \quad (2)$$

149 where k (s⁻¹), V (4×10^{-4} m³), S (9.8×10^{-3} m²) and ω (314.05 m s⁻¹) are the reaction rate
150 constant, the volume of the rectangular reactor, the surface area of the sample dish, and the
151 mean molecular speed of SO₂, respectively.

152 The uptake process of SO₂ on SiO₂ depended on the reaction of SO₂ with SiO₂ and the mass
153 transport of SO₂ to the surface. It can be expressed with the equation 3,

154
$$k'_{\text{r, SiO}_2} = \left[\frac{1}{k_{\text{obs, SiO}_2} - k_{\text{obs, wall}}} - \frac{a}{N_u D} \right]^{-1} \quad (3)$$

155 where $k_{\text{obs, SiO}_2}$ and $k_{\text{obs, wall}}$ (s⁻¹) are the apparent rate constants measured with and without
156 SiO₂ samples, respectively. $k'_{\text{r, SiO}_2}$ is the reaction rate constant of SO₂ accounting for the
157 diffusion effect; D (0.1337 cm² s⁻¹) is the diffusion coefficient of SO₂ in air; a (1 cm) is one
158 half height of the flow reactor; N_u is the Nusselt numbers obtained with a calculation method
159 from Solbrig and Gidaspow (1967), which represents the mass transport. Then, the corrected γ
160 can be calculated by the equation 2 where k was replaced by $k'_{\text{r, SiO}_2}$. In our experiments, the
161 correction for γ was estimated to be approximate 10%. Initial uptake coefficients (γ_0) and
162 steady-state uptake coefficients (γ_s) were calculated by averaging the signals within the 1.0 and
163 40–60 min reaction time, respectively.

164 To understand the diffusion depth of SO₂ and determine the interaction of SO₂ with the
165 underlying layers of SiO₂, the uptake of SO₂ as a function of the SiO₂ mass under irradiation

166 was shown in Figure S6. The γ exhibited a linear increase in the SiO₂ mass range of 0.05–2.0
167 g, while it remained unchanged at the SiO₂ mass > 3.0 g. Therefore, the uptake coefficient of
168 SO₂ in the linear regions was normalized using the BET surface area of SiO₂ by the equation 4
169 (Brunauer et al., 1938),

$$170 \quad \gamma_{\text{BET}} = \frac{S_{\text{geo}} \times \gamma_{\text{geo}}}{S_{\text{BET}} \times m_{\text{SiO}_2}} \quad (4)$$

171 where γ_{BET} is the SO₂ uptake coefficient normalized to the BET surface area; S_{geo} (9.8×10^{-3}
172 m²) is the geometric area of the sample dish; S_{BET} ($0.419 \text{ m}^2 \text{ g}^{-1}$) is the BET surface area of
173 SiO₂; m_{SiO_2} (0.05–2.0 g) is the SiO₂ mass. The same method was also used to calculate the
174 uptake coefficients of SO₂ on other mineral oxides.

175 **2.4 In Situ DRIFTS analysis**

176 The changes in the chemical compositions on mineral oxides in the SO₂ uptake process were
177 investigated by the Fourier transform infrared (FTIR) spectrometer (Thermo Nicolet iS50)
178 equipped with an *in situ* diffuse reflectance accessory and a mercury cadmium telluride (MCT)
179 detector. About 14 mg mineral oxides was placed into a stainless-steel cup inside the reaction
180 cell. To remove adsorbed impurities, SiO₂ was purged with a 150 mL min^{-1} airflow (N₂/O₂
181 volume ratio = 4:1) at RH=40% for 1 h. Then, a background spectrum of unreacted samples
182 was collected. SO₂ (2 ppm) was introduced into the reaction cell, and the IR spectra was
183 recorded as a function of time at a resolution of 4 cm^{-1} by averaging 100 scans. The light from
184 the xenon lamp (500 W) was transmitted into the DRIFTS reaction cell via a fiber. To verify
185 the role of intermediate, Ru(bpy)₃(Cl)₂ and NaHCO₃, acting as ³SO₂ and •OH scavengers
186 (Bulgakov and Safonova, 1996; Gen et al., 2019a), respectively, were mixed with SiO₂ powder
187 in an agate mortar, and the mixture was put in the reaction cell of DRIFTS.

188

189 **3 Results and discussion**

190 **3.1 Photo-enhanced uptake of SO₂**

191 Acting as the most abundant mineral oxides, SiO₂ was firstly used to investigate the uptake
192 behaviors of SO₂. As shown in Figure 1A, when SO₂ (80 ppb) was exposed to SiO₂ in the dark,

193 the SO₂ concentration decreased to 70 ppb, and then it quickly increased and reached the steady
194 state after 20 min. Upon exposure to SiO₂ under irradiation, the SO₂ concentration exhibited a
195 greater drop than that in the dark. The deactivation of SO₂ uptake on SiO₂ was very slight after
196 20 mins under irradiation. These suggest that light can significantly promote the heterogeneous
197 reaction of SO₂ on SiO₂. When SO₂ did not contact with SiO₂, its concentration recovered
198 rapidly. The desorption of SO₂ was observed when SO₂ was isolated from SiO₂ in the dark and
199 under irradiation, indicating that the physical adsorption partially contributed to the SO₂ loss
200 during the photochemical process. The proportion of the desorbed SO₂ during the uptake
201 process can be quantified by dividing the integral of reversible desorption of SO₂ ($t = 80\text{--}100$
202 min) into the integral of the SO₂ uptake ($t = 20\text{--}80$ min), which was calculated to be 95% and
203 12% in the dark and under irradiation, respectively. This implies that SO₂ uptake in the dark
204 was primarily ascribed to the physical adsorption of SO₂, while SO₂ uptake under irradiation
205 was mainly attributed to chemical processes or irreversible adsorption.

206 The uptake coefficients of SO₂ on SiO₂ as a function of irradiation intensity were shown in
207 Figure 1B. The errors in all figures are the standard deviations of three repetitive experiments.
208 Both $\gamma_{0, \text{BET}}$ and $\gamma_{s, \text{BET}}$ displayed a well linear relationship with the irradiation intensity, further
209 confirming the photochemical nature for the reactions of SO₂ on SiO₂. In particular, $\gamma_{0, \text{BET}}$ and
210 $\gamma_{s, \text{BET}}$ on SiO₂ under simulated solar irradiation was comparable with those ($10^{-7}\text{--}10^{-6}$) on
211 Gobi Desert dust (GDD) and Arizona Test Dust (ATD) under UV irradiation, which contained
212 photocatalytic metal oxides (Park et al., 2017). As for the SO₂ uptake on TiO₂, $\gamma_{0, \text{BET}}$ and $\gamma_{s, \text{BET}}$
213 were measured to be 10^{-6} and 10^{-7} , respectively, by using the flow tube (Ma et al., 2019), which
214 were similar to our results. It should be pointed out that the similar uptake coefficient did not
215 mean the comparable ability of photoactive and non-photoactive mineral oxides to SO₂ uptake,
216 since the uptake coefficient was highly dependent on environmental conditions (SO₂
217 concentration, relative humidity, mineral oxides mass, light source and pressure) and reactor
218 type (chamber and flow tube reactor), and the uptake coefficients mentioned here were not
219 obtained under the exact same reaction conditions used in our study. The purities of different

220 mineral substances are 95%–98%. If photoactive impurities mainly contributed to the SO₂
 221 uptake in the experiment, the SO₂ uptake coefficient on impurities should be 20–50 times
 222 higher than the current SO₂ uptake coefficient and range from 10⁻⁵ to 10⁻³. The SO₂ uptake
 223 coefficient on photoactive substances was reported to be 10⁻⁷–10⁻⁶ in previous studies (Ma et
 224 al., 2019; Park et al., 2017). Thus, the impurities in minerals were less likely responsible for
 225 the SO₂ uptake.

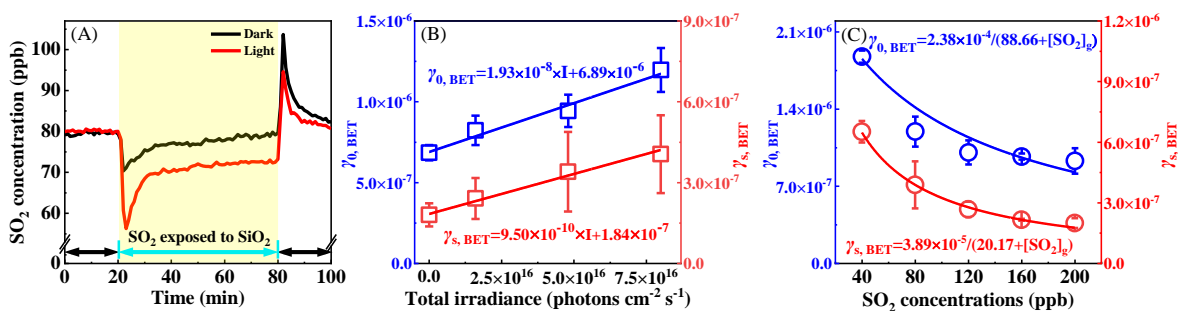
226 Figure 1C shows the evolution of $\gamma_{0, \text{BET}}$ and $\gamma_{s, \text{BET}}$ at different SO₂ concentrations under
 227 irradiation. An inverse dependence of $\gamma_{0, \text{BET}}$ and $\gamma_{s, \text{BET}}$ on the SO₂ concentration was observed,
 228 meaning that both initial and steady-state uptake reactions were lower efficient at higher SO₂
 229 concentrations. The uptake of gases on the solid surfaces usually follows the Langmuir-
 230 Hinshelwood (L-H) mechanism (Ammann et al., 2003; Zhang et al., 2020b), suggesting that
 231 gaseous molecules are quickly absorbed on the surfaces, and then the reactions occur among
 232 the absorbed species. Assuming that the adsorption of SO₂ on SiO₂ is in accord with the
 233 Langmuir isotherm, the dependence of γ on the SO₂ concentration can be described by the
 234 equation 5 (Zhang et al., 2020b),

$$235 \gamma = \frac{(4V/S\omega)k[\text{SiO}_2]_{\text{T}}K_{\text{SO}_2}}{1+K_{\text{SO}_2}[\text{SO}_2]_{\text{g}}} \quad (5)$$

236 where [SO₂]_g is the concentration of gaseous SO₂; [SiO₂]_T is the total number of active sites
 237 on SiO₂; k is the reaction rate constant of SO₂ absorbed on SiO₂; K_{SO_2} represents the Langmuir
 238 adsorption constant of SO₂. Because the SiO₂ mass remained constant during the reaction, the
 239 equation 5 can be written as the equation 6,

$$240 \gamma = \frac{a}{1 + K_{\text{SO}_2}[\text{SO}_2]_{\text{g}}} \quad (6)$$

241 where $a=(4V/S\omega)k[\text{SiO}_2]_{\text{T}}K_{\text{SO}_2}$. As shown in Figure 1C, the equation 6 can well describe the
 242 correlation of the SO₂ uptake coefficient with the SO₂ concentration, suggesting that the L-H
 243 mechanism can explain the influence of the SO₂ concentration on $\gamma_{0, \text{BET}}$ and $\gamma_{s, \text{BET}}$.



244

245 **Figure 1.** (A) The temporal variation of the SO₂ concentration on SiO₂ in the dark and under
 246 irradiation (7.93×10^{16} photons cm⁻² s⁻¹); The background changes of the SO₂ concentration

247 in the blank reactor have been deducted. (B) The $\gamma_{0, \text{BET}}$ and $\gamma_{s, \text{BET}}$ of SO₂ on SiO₂ as a

248 function of the light intensity. (C) The $\gamma_{0, \text{BET}}$ and $\gamma_{s, \text{BET}}$ of SO₂ on SiO₂ at different SO₂

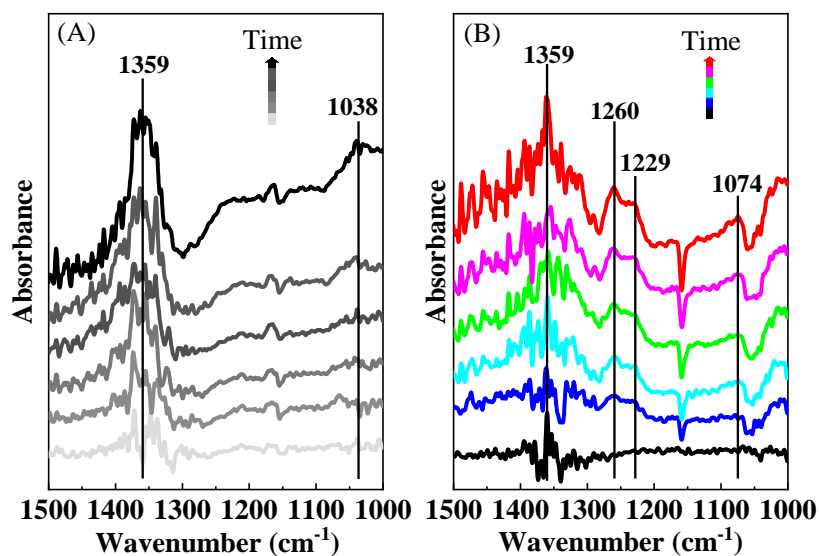
249 concentrations under irradiation (7.93×10^{16} photons cm⁻² s⁻¹); The fitting lines for $\gamma_{0, \text{BET}}$

250 and $\gamma_{s, \text{BET}}$ were based on the Langmuir-Hinshelwood mechanism using equation 6. Reaction

251 conditions: SiO₂ mass of 0.2 g, temperature of 298 K, RH of 40% and O₂ content of 20%.

252 3.2 Photo-induced formation of sulfates by the SO₂ uptake

253 To investigate the products formed on SiO₂, *in situ* DRIFTS spectra were recorded, as shown
 254 in Figure 2. The band at 1359 cm⁻¹ was assigned to physically-adsorbed SO₂ on SiO₂ (Urupina
 255 et al., 2019). The bidentate sulfate and bisulfate contributed to the bands at 1260 and 1229/1074
 256 cm⁻¹ (Urupina et al., 2019; Yang et al., 2020), respectively. The bands at 1038 cm⁻¹ may be
 257 related to the monodentate sulfite (Yang et al., 2019; Wang et al., 2019). It was noted that the
 258 intensity of physically-adsorbed SO₂ (1359 cm⁻¹) under irradiation was lower than that in the
 259 dark (Figure S7), which may be ascribed to further conversion of SO₂ absorbed on SiO₂ under
 260 irradiation. Especially, the sulfate bands (1260, 1229 and 1074 cm⁻¹) only appeared under
 261 irradiation, while the sulfites (1038 cm⁻¹) were only detected in the dark. This suggests that
 262 light changed the SO₂ conversion pathways on SiO₂. As shown in Figure S7, the bands at
 263 1157/1055 cm⁻¹ were assigned to the asymmetric stretching of Si-O (Hu et al., 2003). Sulfate
 264 generated on the surface may interact with SiO₂, leading to a decrease in the intensity of peaks
 265 (1157/1055 cm⁻¹).



266

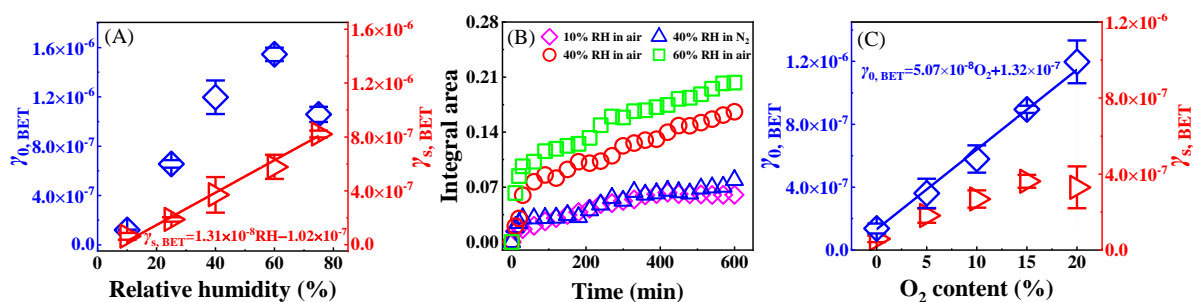
267 **Figure 2.** *In situ* DRIFTS spectra of SiO₂ during the uptake process of SO₂ (2 ppm) in the
 268 dark (A) and under irradiation (B). Reaction conditions: RH of 40%, temperature of 298 K
 269 and O₂ content of 20%.

270 3.3 Key roles of H₂O and O₂ in photochemical conversion of SO₂ to sulfates

271 Figure S8A shows temporal variations of the SO₂ concentration in the reaction with SiO₂ at
 272 RH=10% and 60% under irradiation. The uptake of SO₂ was very weak at RH=10%, whereas
 273 it was obvious at RH=60%. Moreover, H₂O markedly prolonged the time to reach the steady-
 274 state uptake of SO₂. This definitely determines that H₂O plays a distinct enhancement role in
 275 the photochemical uptake of SO₂. As shown in Figure 3A, $\gamma_{0, \text{BET}}$ had a continuous increase
 276 from $(1.20 \pm 0.04) \times 10^{-7}$ to $(1.54 \pm 0.07) \times 10^{-6}$ with increasing the RH in the 10%–60% range,
 277 but it decreased to $(1.05 \pm 0.09) \times 10^{-6}$ at RH=75%. The $\gamma_{s, \text{BET}}$ linearly depended on the RH,
 278 and linear fitting to $\gamma_{s, \text{BET}}$ versus RH yielded the equation $\gamma_{s, \text{BET}} = 1.31 \times 10^{-8} \times \text{RH} - 1.02 \times 10^{-7}$.
 279 Adsorbed H₂O promoted the hydration and dissociation of SO₂ (Huang et al., 2015), and it may
 280 generate reactive oxygen species (ROS) such as •OH or HO₂ radicals to oxidize SO₂ under
 281 irradiation (Li et al., 2020; Ma et al., 2019), which would lead to positive effects of RH on the
 282 SO₂ uptake. Adsorbed H₂O also occupied adsorptive and active sites on the surface, and
 283 produced the competition with SO₂. When this competitive role was dominated, the uptake of

284 SO₂ would be hindered.

285 The DRIFTS spectra of SiO₂ during the SO₂ uptake at different RHs are shown in Figure
286 S9A. The band intensities of sulfates (1260 and 1229 cm⁻¹) at RH=60% were greatly stronger
287 than those at RH=10%, suggesting that H₂O significantly promotes the sulfate formation. To
288 further investigate the influence of H₂O on the sulfate formation, the integrated area of sulfates
289 in the DRIFTS spectra (1289–1202 cm⁻¹) as a function of the time at different RHs is illustrated
290 in Figure 3B. Sulfates exhibited a fast formation in the initial 30 min at any RH, and then they
291 were continuously generated at a relatively slow rate. Absorptive sites for SO₂ can be blocked
292 because of the accumulation of H₂O and products (sulfites and sulfates), resulting in the gradual
293 deactivation of the surface. It was noted that sulfates had a more distinct formation trend with
294 increasing the RH, revealing that H₂O can act as an important participator in the production of
295 sulfates by the photochemical uptake of SO₂ on SiO₂.



296

297 **Figure 3.** (A) The dependence of $\gamma_{0, \text{BET}}$ and $\gamma_{s, \text{BET}}$ on RH. (B) Integrated area of sulfates in
298 DRIFTS spectra (1289–1202 cm⁻¹) as a function of time. (C) The dependence of $\gamma_{0, \text{BET}}$ and
299 $\gamma_{s, \text{BET}}$ on O₂. Reaction conditions: SiO₂ mass of 0.2 g, irradiation intensity of 7.93×10^{16}
300 photons cm⁻² s⁻¹, temperature of 298 K, O₂ content of 20% for (A) and RH of 40% for (B).

301 Figure S8B displays effects of O₂ on the photochemical uptake of SO₂ on SiO₂. Negligible
302 SO₂ uptake occurred in N₂, while there was a significant decrease in the SO₂ concentration in
303 air. The $\gamma_{0, \text{BET}}$ greatly increased from $(1.37 \pm 0.45) \times 10^{-7}$ in N₂ to $(1.19 \pm 0.13) \times 10^{-6}$ in 20%
304 O₂ (Figure 3C), confirming that O₂ was involved in the reaction of SO₂ on SiO₂. The $\gamma_{s, \text{BET}}$

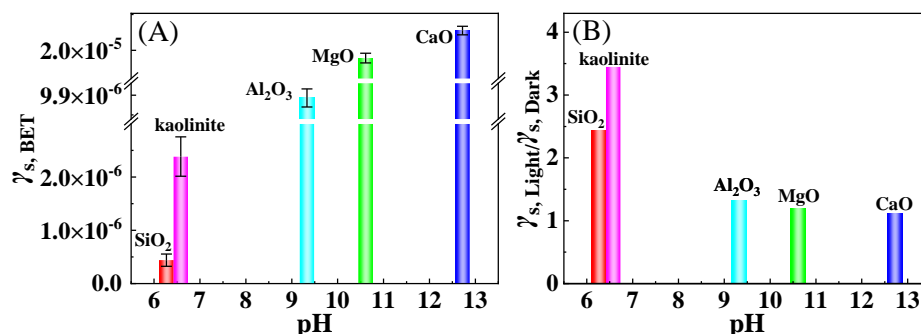
305 displayed different dependence behaviors on O₂. It exhibited an increase from $(7.10 \pm 2.85) \times$
306 10^{-8} in N₂ to $(4.37 \pm 0.58) \times 10^{-7}$ in 15% O₂, whereas it remained unchanged in 20% O₂.

307 DRIFTS spectra of SiO₂ during the SO₂ uptake in N₂ and air was compared in Figure S9B.
308 In both air and N₂, the bands of absorbed SO₂ (1359 cm⁻¹), sulfates (1260, 1229 and 1074
309 cm⁻¹). Nevertheless, their intensities in N₂ were weaker than those in air. According to the
310 integrated area of sulfates in the DRIFTS spectra (1289–1202 cm⁻¹) as a function of time, the
311 formation trends of sulfates were similar in N₂ and air (Figure 3B), while the sulfate formation
312 rate in N₂ was obviously lower than that in air, meaning that O₂ enhanced the sulfate production.
313 It was reported that the production rate of sulfates from the SO₂ uptake on TiO₂ and by the
314 photolysis of nitrates under UV irradiation in N₂ was also smaller than that in air (Ma et al.,
315 2019; Gen et al., 2019b). In addition, it was noted that sulfates can be generated in N₂, meaning
316 that O₂ was not necessary and some pathways contributed to sulfates without O₂.

317 **3.4 Ubiquitously photoenhanced conversion of SO₂ to sulfates**

318 To better assess the potential for photochemical conversion of SO₂ to sulfates, the SO₂ uptake
319 experiments were further performed for typical mineral oxides without photocatalytic activity.
320 As displayed in Figure S10, more obvious uptake behaviors of SO₂ on kaolinite, Al₂O₃, MgO
321 and CaO were observed under irradiation when compared to those in the dark. Figure 4A shows
322 that there was the largest $\gamma_{s, \text{BET}}$ for CaO among five minerals, and $\gamma_{s, \text{BET}}$ positively depended
323 on the basicity (pH) of mineral oxides. Basic oxides generally contains more surface hydroxyls,
324 which is in favor of sulfite and sulfate formation to enhance the heterogeneous uptake of SO₂
325 (Zhang et al., 2006). The ratios of steady-state uptake coefficients under irradiation to those in
326 the dark ($\gamma_{s, \text{Light}}/\gamma_{s, \text{Dark}}$) were larger than 1.0 for all mineral oxides (Figure 4B). The
327 experiments for the pH dependence on SiO₂ have been also performed (Figure S11). The pH
328 of SiO₂ suspension was adjusted to pH = 9, and $\gamma_{s, \text{BET}}$ and $\gamma_{s, \text{Light}}/\gamma_{s, \text{Dark}}$ were determined to
329 be $(8.79 \pm 0.85) \times 10^{-6}$ and 1.31, respectively. These results suggest that light can generally
330 enhance the SO₂ uptake on minerals at a wide pH range. However, the $\gamma_{\text{Light}}/\gamma_{\text{Dark}}$ had smaller
331 values with an increase in the basicity, suggesting that the promotion effect of the light was less

332 remarkable for basic oxides.



333

334 **Figure 4.** (A) The dependence of $\gamma_{s, \text{BET}}$ under irradiation on the basicity (pH) of mineral

335 oxides. (B) The ratios of steady-state uptake coefficients under irradiation to those in the dark

336 ($\gamma_{s, \text{Light}} / \gamma_{s, \text{Dark}}$). Reaction conditions: mineral oxides mass of 0.2 g, irradiation intensity of

337 7.93×10^{16} photons $\text{cm}^{-2} \text{s}^{-1}$, temperature of 298 K, RH of 40% and O₂ content of 20%.

338 As shown in Figure 5A and B, the band at 1300 cm^{-1} should be ascribed to the sulfate. The

339 intensity of sulfate (1300 and 1220 cm^{-1}) under irradiation was larger than those in the dark.

340 Compared to weaker peaks of sulfates (1200 and 1260 cm^{-1}) for Al₂O₃ in the dark (Figure 5C),

341 a stronger band of bisulfates appeared at 1220 cm^{-1} under irradiation (Figure 5D). By contrast

342 to the generation of sulfates for kaolinite and Al₂O₃, both sulfites and sulfates formations were

343 observed for MgO and CaO (Figure 5E–H). Sulfites were dominant in the dark, as shown by

344 the peaks at 966 and 1020 cm^{-1} for MgO and 943 cm^{-1} for CaO, whereas the sulfate formation

345 was significantly enhanced under irradiation according to peak intensities at 1163 cm^{-1} for

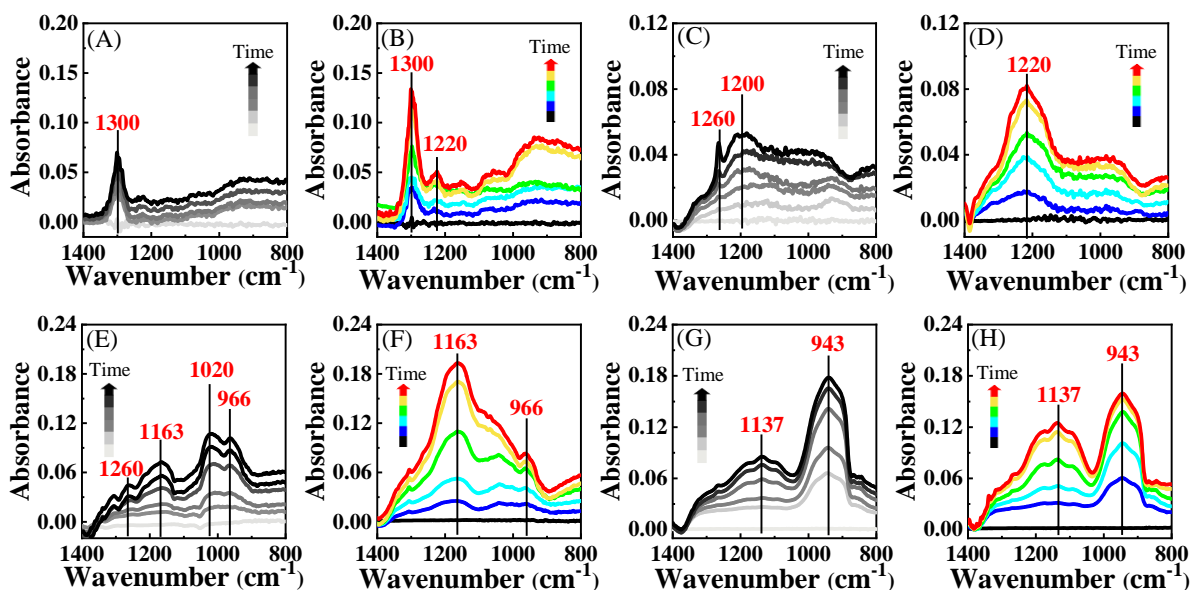
346 MgO and 1137 cm^{-1} for CaO. It should be noted that these mineral oxides were non-

347 photoactive because of their poor light absorption property (Figure S1). Nevertheless, it was

348 very surprised that the light can greatly promote the formation of sulfates via the SO₂ uptake

349 process on mineral oxides without photocatalytic activity, which was strongly suggested to be

350 a new and important finding for atmospheric sulfate sources.



351
 352 **Figure 5.** *In situ* DRIFTS spectra of kaolinite (A and B), Al₂O₃ (C and D), MgO (E and F),
 353 CaO (G and H) during the uptake process of SO₂ (2 ppm) for 600 min in the dark (black
 354 lines) and under irradiation (colorful lines). Reaction conditions: RH of 40%, temperature of
 355 298 K and O₂ content of 20%.

356 3.5 Conversion mechanisms of SO₂ to sulfates

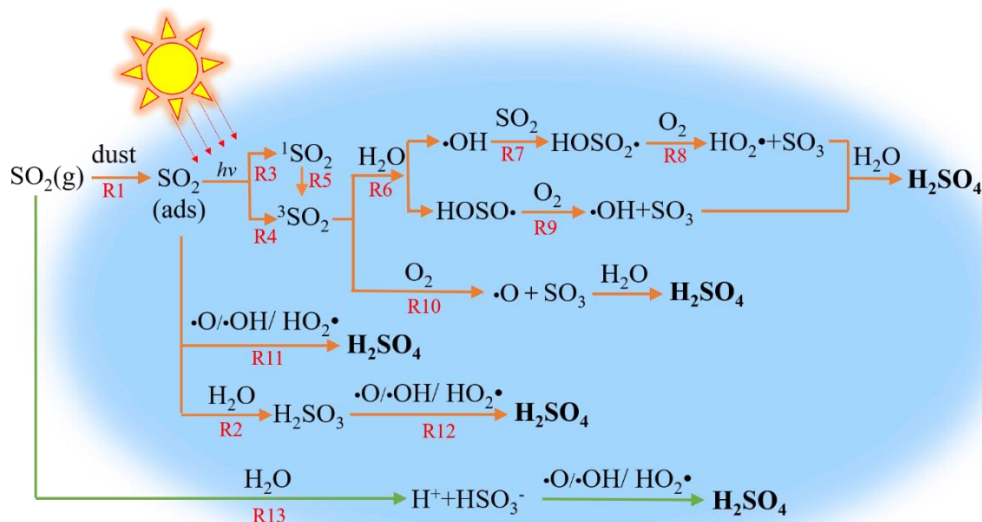
357 Heterogeneous photochemical reaction mechanisms of SO₂ on non-photoactive mineral dust
 358 were proposed in light of experimental observations (Figure 6). Gaseous SO₂ was adsorbed on
 359 the surface (R1), and then reacted with H₂O to form sulfites (R2). Under irradiation, adsorbed
 360 SO₂ accepted photons to form its singlet states (¹SO₂) and ³SO₂ (R3–5) (Sidebottom et al., 1972;
 361 Martins-Costa et al., 2018). The reaction between ³SO₂ and H₂O resulted in the formation of
 362 HOSO• and •OH (R6), which can combine with SO₂ to produce HOSO₂• (R7). HOSO• and
 363 HOSO₂• can be transformed into SO₃, which reacted with H₂O to drive the sulfate formation
 364 (R8 and R9). The interaction between ³SO₂ and O₂ may also generate SO₃ directly, which
 365 would be converted to sulfates subsequently (R10). Theoretical calculations suggested that the
 366 multistep reactions between ³SO₂ with H₂O and O₂ had small energy barriers or were barrier-
 367 free (Gong et al., 2022), which could enhance the generation of ROS and the transformation of
 368 S(IV) to S(VI). As displayed by R11 and R12, SO₂ and H₂SO₃ adsorbed on the surface may be
 369 oxidized to form sulfates via the reactions with ROS including •O, •OH or HO₂•, which were

370 produced in R6 and R8–10. In addition, gaseous SO₂ could be dissolved into adsorbed H₂O to
371 generate bisulfites, which would be finally converted to sulfates by ROS (R13) (Urupina et al.,
372 2019). As displayed in Figure S12A, the IR peaks of sulfates were not observed when tris (2,2'-
373 bipyridine) ruthenium dihydrochloride (Ru(bpy)₃(Cl)₂) was employed as the quencher of ³SO₂.
374 The peaks were assigned to the vibrations of excited Ru(bpy)₃(Cl)₂ (Mukuta et al., 2014). This
375 definitely proves that ³SO₂ is the key trigger for the sulfate formation. Figure S12B shows that
376 the peaks of sulfates were obviously weaker in the presence of NaHCO₃, confirming the
377 dominant contribution of •OH formed in R6 and R9 to the formation of sulfates.

378 Several photochemical mechanisms have been reported to explain the sulfate formation via
379 the SO₂ uptake on various surfaces. Photoactive mineral oxides (such as TiO₂, F₂O₃ and ZnO)
380 can accept photons to produce electron-hole pairs, which generated ROS for the conversion of
381 SO₂ to sulfates (Ma et al., 2019; Li et al., 2019; Wang et al., 2020b). For example, •OH and
382 HO₂•, generated from the reaction of hole with H₂O and electron with O₂, respectively, can act
383 as oxidizing agents for the reaction with SO₂ (Ma et al., 2019). Similarly, the reaction of SO₂
384 with photo-induced •OH obviously enhanced the formation of sulfate on diesel soot and actual
385 PM_{2.5} (Zhang et al., 2022; Zhang et al., 2020c). NO₂ and NO₂⁻/HNO₂ can be formed in the
386 nitrates photolysis, and primarily contributed to the oxidation of SO₂ to sulfates on nitrates (Gen
387 et al., 2019b; Gen et al., 2019a). Theoretically, the mechanism proposed in this study should
388 also occur on photo-excited substrates. Taking TiO₂ as an example, SO₂ competed with TiO₂
389 for photons, and the production efficiency of ³SO₂ and excited state of TiO₂ (TiO₂^{*}) depended
390 on their light absorption properties. Meanwhile, ³SO₂ had a competition electron-hole pairs
391 generated from TiO₂^{*} for O₂ and H₂O. Thus, the dominant mechanism for the SO₂ uptake on
392 TiO₂ should be related to light absorption properties of precursors and the reactivity for ³SO₂
393 and TiO₂^{*} to O₂ and H₂O. By contrast, all mineral oxides used here cannot be excited under
394 irradiation according to their light absorption spectra (Figure S1). Nevertheless, SO₂ adsorbed
395 on mineral oxides can absorb the ultraviolet radiation (290–400 nm) to form the excited states
396 of SO₂ (SO₂^{*}) (Kroll et al., 2018), which subsequently reacted with H₂O and O₂, finally
397 converting SO₂ to sulfates. The SO₂ uptake experiment in the dark and the visible light (>420

398 nm) was carried out (Figure S13). An ignorable difference was observed for the SO₂
 399 concentration with or without visible light, suggesting that visible light had a minor contribution
 400 to the photoenhanced SO₂ uptake.

401 According to the experimental results, some surfaces, providing absorptive sites for SO₂, can
 402 enhance the photooxidation of SO₂ to sulfates. However, the promotion effect would vary with
 403 different substances. For example, the current experiments on some basic minerals indicate that
 404 light plays a minor enhancement role in the SO₂ uptake (Figure 4), but it could still enhance the
 405 sulfate formation (Figure 5). The solubility and effective Henry's law constant of SO₂ were
 406 positively dependent on pH. Thus, SO₂ was more liable to be dissolved to form HSO₃⁻/SO₃²⁻
 407 on more alkaline surface, leading to a strong SO₂ uptake in the dark (Figure 4A and 4B), and
 408 abundant sulfites on surfaces (Figure 5). Nevertheless, gaseous SO₂ tends to be adsorbed on
 409 kaolinite and Al₂O₃ due to less solubility of SO₂ on these surfaces, and then converted to sulfate
 410 under irradiation (Figure 6). Accordingly, a strong promotion effect of light on SO₂ uptake was
 411 observed on neutral and weakly alkaline surfaces (Figure 4B).



412
 413 **Figure 6.** The proposed photochemical conversion mechanisms of SO₂ to sulfates on non-
 414 photoactive mineral dust.

415 4 Atmospheric implications

416 The lifetime (τ) for photochemical loss of SO₂ on mineral dust was given using the equation

417 7,

$$418 \quad \tau = \frac{4}{\gamma\omega A} \quad (7)$$

419 where γ and ω are the uptake coefficient and the mean molecular speed of SO_2 , respectively; A
420 is the surface area density of mineral dust, and it is estimated to be $(1.4\text{--}4.8) \times 10^{-5} \text{ cm}^2 \text{ cm}^{-3}$
421 (Zhang et al., 2019; He et al., 2018b). In this work, $\gamma_{s, \text{BET}}$ of SO_2 on several mineral oxides
422 were measured to be from 4.39×10^{-7} to 3.45×10^{-5} under conditions with SO_2 concentration
423 of 40 ppb, irradiation intensity of $7.93 \times 10^{16} \text{ photons cm}^{-2} \text{ s}^{-1}$ and RH of 40%. Thus, the τ of
424 SO_2 with respect to the photooxidation on mineral dust was calculated to be 0.9–240 days,
425 which was shorter than that (54 years) for the photochemical uptake of SO_2 on TiO_2 and the
426 corresponding one (346 days) for the heterogeneous oxidation of SO_2 on ATD in the presence
427 of nitrates (Ma et al., 2019; Zhang et al., 2019). The reaction conditions in this study and those
428 in the literatures are different in some respects, and the previously reported SO_2 uptake
429 coefficient ($10^{-7}\text{--}10^{-6}$) had a lower value (Ma et al., 2019). The huge difference in the τ of SO_2
430 was also ascribed to the variation in the surface area density. The content of TiO_2 in mineral
431 dust was only about 1%, and thus the surface area density of TiO_2 was about $10^{-7} \text{ cm}^2 \text{ cm}^{-3}$,
432 leading to a longer τ (54 years) for SO_2 on TiO_2 (Ma et al., 2019). It was comparable to the
433 lifetime (3.6–20 days) of SO_2 for the gas-phase reaction with $\bullet\text{OH}$ at a concentration of $\sim 10^{-6}$
434 molecules cm^{-3} (Huang et al., 2015; Zhang et al., 2019). Therefore, the photochemical process
435 with the excited state SO_2 acting as a driver on mineral dust was an important pathway for the
436 SO_2 sink in the atmosphere.

437 Sulfates show significant influences on the atmosphere, such as an important contributor to
438 the haze formation, affecting the activity of aerosols acting as cloud condensation nuclei (CCN)
439 and ice nuclei (IN), and modifying optical property and acidity of aerosols. A sulfate formation
440 rate (R) can be obtained using γ by the equation 8 (Cheng et al., 2016),

$$441 \quad R = \frac{d[\text{SO}_4^{2-}]}{dt} = \left[\frac{R_p}{D} + \frac{4}{\gamma\omega} \right]^{-1} A[\text{SO}_2] \quad (8)$$

442 where R_p is the radius of mineral dust, which can be estimated using the equation 9 (Li et al.,

443 2020),

$$444 R_p = (0.254 \times [\text{PM}_{2.5}]/(\mu\text{g m}^{-3}) + 10.259) \times 10^{-9} \text{ m} \quad (9)$$

445 where $[\text{PM}_{2.5}]$ was average $\text{PM}_{2.5}$ mass concentration, and $300 \mu\text{g m}^{-3}$ was used for the polluted
446 periods in typical China cities (Li et al., 2020; Guo et al., 2014). It was assumed that mineral
447 dust accounted for 50% mass of $\text{PM}_{2.5}$ (Tohidi et al., 2022), and the mass fraction of SiO_2 ,
448 Al_2O_3 , MgO , and CaO in mineral dust was 60%, 12.5%, 4% and 6.5%, respectively (Urupina
449 et al., 2021; Urupina et al., 2019; Usher et al., 2003). Thus, R was determined to be $2.15 \mu\text{g}$
450 $\text{m}^{-3} \text{h}^{-1}$. This suggests that the SO_2 on non-photoactive surfaces is a newly identified sulfate
451 formation pathway in some dust-rich conditions.

452

453 **Author contributions**

454 CH, WY and JM designed and conducted experiments; CH, WY and JM analyzed the data and
455 prepared the paper with contributions from HY; FL conducted experiments; CH supervised the
456 project.

457

458 **Competing interests**

459 The authors declare that they have no conflict of interest.

460

461 **Acknowledgements**

462 This work was supported by the National Natural Science Foundation of China [grant number
463 42077198], the LiaoNing Revitalization Talents Program [grant number XLYC1907185], and
464 the Fundamental Research Funds for the Central Universities [grant numbers N2325034;
465 N2025011].

466

467 **Reference**

468 Adams, J., Rodriguez, D., and Cox, R.: The uptake of SO_2 on Saharan dust: A flow tube study,
469 *Atmos. Chem. Phys.*, 5, 2679-2689, <https://doi.org/10.5194/acpd-5-2643-2005>, 2005.
470 Alexander, B., Park, R. J., Jacob, D. J., and Gong, S.: Transition metal-catalyzed oxidation of
471 atmospheric sulfur: Global implications for the sulfur budget, *J. Geophys. Res.*, 114, 2309-

2312, <https://doi.org/10.1029/2008jd010486>, 2009.

Ammann, M., Poschl, U., and Rudich, Y.: Effects of reversible adsorption and Langmuir-Hinshelwood surface reactions on gas uptake by atmospheric particles, *Phys. Chem. Chem. Phys.*, 5, 351-356, <https://doi.org/10.1039/b208708a>, 2003.

Bounechada, D., Anderson, D., Skoglundh, M., and Carlsson, P.: SO₂ adsorption on silica supported iridium, *J. Chem. Phys.*, 146, 084701-084708, <https://doi.org/10.1063/1.4976835>, 2017.

Brunauer, B., Deming, L., Deming, W., and Teller, E.: Adsorption of gases in multimolecular layers, *J. Am. Chem. Soc.*, 60, 309-319, <https://doi.org/10.1021/ja01269a023>, 1938.

Bulgakov, R. G. and Safonova, L. A.: Chemiluminescence in the oxidation of Na₂S by oxygen in water solutions, *Russ. Chem. Bull.*, 45, 1775-1776, <https://doi.org/10.1007/bf01431827>, 1996.

Cao, J., Tie, X., Dabberdt, W. F., Jie, T., Zhao, Z., An, Z., Shen, Z., and Feng, Y.: On the potential high acid deposition in northeastern China, *J. Geophys. Res.: Atmos.*, 118, 4834-4846, <https://doi.org/10.1002/jgrd.50381>, 2013.

Chan, M. and Chan, C.: Hygroscopic properties of two model humic-like substances and their mixtures with inorganics of atmospheric importance, *Environ. Sci. Technol.*, 37, 5109-5115, <https://doi.org/10.1021/es034272o>, 2003.

Chen, Y., Tong, S., Li, W., Liu, Y., Tan, F., Ge, M., Xie, X., and Sun, J.: Photocatalytic oxidation of SO₂ by TiO₂: Aerosol formation and the key role of gaseous reactive oxygen species, *Environ. Sci. Technol.*, 55, 9784-9793, <https://doi.org/10.1021/acs.est.1c01608>, 2021.

Cheng, Y., Zheng, G., Wei, C., Mu, Q., Zheng, B., Wang, Z., Gao, M., Zhang, Q., He, K., Carmichael, G., Pöschl, U., and Su, H.: Reactive nitrogen chemistry in aerosol water as a source of sulfate during haze events in China, *Sci. Adv.*, 2, 1601530-1601540, <https://doi.org/10.1126/sciadv.1601530>, 2016.

Chu, B., Wang, Y. L., Yang, W. W., Ma, J. Z., Ma, Q. X., Zhang, P., Liu, Y. C., and He, H.: Effects of NO₂ and C₃H₆ on the heterogeneous oxidation of SO₂ on TiO₂ in the presence or absence of UV-Vis irradiation, *Atmos. Chem. Phys.*, 19, 14777-14790, <https://doi.org/10.5194/acp-19-14777-2019>, 2019.

Davis, D. D., Ravishankara, A. R., and Fischer, S.: SO₂ oxidation via the hydroxyl radical: Atmospheric fate of HSO_x radicals, *Geo. Res. Lett.*, 6, 113-116, <https://doi.org/10.1029/GL006i002p00113>, 1979.

Dentener, F., Carmichael, G., Zhang, Y., Lelieveld, J., and Crutzen, P.: Role of mineral aerosol as a reactive surface in the global troposphere, *J. Geophys. Res.: Atmos.*, 101, 22869-22889, <https://doi.org/10.1029/96jd01818>, 1996.

Gen, M., Zhang, R., Huang, D., Li, Y., and Chan, C.: Heterogeneous oxidation of SO₂ in sulfate production during nitrate photolysis at 300 nm: Effect of pH, relative humidity, irradiation intensity, and the presence of organic compounds, *Environ. Sci. Technol.*, 53, 8757-8766, <https://doi.org/10.1021/acs.est.9b01623>, 2019a.

Gen, M., Zhang, R., Huang, D., Li, Y., and Chan, C.: Heterogeneous SO₂ oxidation in sulfate formation by photolysis of particulate nitrate, *Environ. Sci. Tech. Lett.*, 6, 86-91, <https://doi.org/10.1021/acs.estlett.8b00681>, 2019b.

514 Golobokova, L., Khodzher, T., Khuriganova, O., Marinayte, I., Onishchuk, N., Rusanova, P.,
515 and Potemkin, V.: Variability of chemical properties of the atmospheric aerosol above lake
516 baikal during large wildfires in siberia, *Atmosphere*, 11, 1230-1250,
517 <https://doi.org/10.3390/atmos11111230>, 2020.

518 Gong, C., Yuan, X., Xing, D., Zhang, D., Martins-Costa, M. T. C., Anglada, J. M., Ruiz-Lopez,
519 M. F., Francisco, J. S., and Zhang, X.: Fast sulfate formation initiated by the spin-forbidden
520 excitation of SO₂ at the air-water interface, *J. Am. Chem. Soc.*, 144, 22302-22308,
521 <https://doi.org/10.1021/jacs.2c10830>, 2022.

522 Goodman, A., Li, P., Usher, C., and Grassian, V.: Heterogeneous uptake of sulfur dioxide on
523 aluminum and magnesium oxide particles, *J. Phys. Chem. A* 105, 6109-6120,
524 <https://doi.org/10.1021/jp004423z>, 2001.

525 Guo, S., Hu, M., Zamora, M. L., Peng, J., Shang, D., Zheng, J., Du, Z., Wu, Z., Shao, M., Zeng,
526 L., Molina, M. J., and Zhang, R.: Elucidating severe urban haze formation in China, *Proc.*
527 *Natl. Acad. Sci. U. S. A.*, 111, 17373-17378, <https://doi.org/10.1073/pnas.1419604111>,
528 2014.

529 Harris, E., Sinha, B., van Pinxteren, D., Tilgner, A., Fomba, K. W., Schneider, J., Roth, A.,
530 Gnauk, T., Fahlbusch, B., Mertes, S., Lee, T., Collett, J., Foley, S., Borrmann, S., Hoppe, P.,
531 and Herrmann, H.: Enhanced role of transition metal ion catalysis during in-cloud oxidation
532 of SO₂, *Science*, 340, 727-730, <https://doi.org/10.1126/science.1230911>, 2013.

533 He, G., Ma, J., and He, H.: Role of carbonaceous aerosols in catalyzing sulfate formation, *ACS*
534 *Catal.*, 8, 3825-3832, <https://doi.org/10.1021/acscatal.7b04195>, 2018a.

535 He, H., Li, C., Loughner, C. P., Li, Z., Krotkov, N. A., Yang, K., Wang, L., Zheng, Y., Bao, X.,
536 Zhao, G., and Dickerson, R. R.: SO₂ over central China: Measurements, numerical
537 simulations and the tropospheric sulfur budget, *J. Geophys. Res.: Atmos.*, 117, 37-51,
538 <https://doi.org/10.1029/2011jd016473>, 2012.

539 He, P., Alexander, B., Geng, L., Chi, X., Fan, S., Zhan, H., Kang, H., Zheng, G., Cheng, Y., Su,
540 H., Liu, C., and Xie, Z.: Isotopic constraints on heterogeneous sulfate production in Beijing
541 haze, *Atmos. Chem. Phys.*, 18, 5515-5528, <https://doi.org/10.5194/acp-18-5515-2018>,
542 2018b.

543 Herrmann, H., Ervens, B., Jacobi, H. W., Wolke, R., Nowacki, P., and Zellner, R.: CAPRAM_{2.3}:
544 A chemical aqueous phase radical mechanism for tropospheric chemistry, *J. Atmos. Chem.*,
545 36, 231-284, <https://doi.org/10.1023/A:1006318622743>, 2000.

546 Huang, L., Zhao, Y., Li, H., and Chen, Z.: Kinetics of heterogeneous reaction of sulfur dioxide
547 on authentic mineral dust: Effects of relative humidity and hydrogen peroxide, *Environ. Sci.*
548 *Technol.*, 49, 10797-10805, <https://doi.org/10.1021/acs.est.5b03930>, 2015.

549 Hu, Q., Suzuki, H., Gao, H., Araki, H., Yang, W., and Noda, T.: High-frequency FTIR
550 absorption of SiO₂/Si nanowires, *Chem. Phys. Lett.*, 378, 299-304,
551 <https://doi.org/10.1016/j.cplett.2003.07.015>, 2003.

552 Knopf, D., Cosman, L., Mousavi, P., Mokamati, S., and Bertram, A.: A novel flow reactor for
553 studying reactions on liquid surfaces coated by organic monolayers: Methods, validation,
554 and initial results, *J. Phys. Chem. A*, 111, 11021-11032, <https://doi.org/10.1021/jp075724c>,
555 2007.

556 Kroll, J., Frandsen, B., Kjaergaard, H., and Vaida, V.: Atmospheric hydroxyl radical source:
557 Reaction of triplet SO₂ and water, *J. Phys. Chem. A*, 122, 4465-4469, <https://doi.org/10.10>
558 [21/acs.jpca.8b03524](https://doi.org/10.1021/acs.jpca.8b03524), 2018.

559 Langhammer, D., Kullgren, J., and Osterlund, L.: Photoinduced adsorption and oxidation of
560 SO₂ on anatase TiO₂, *J. Am. Chem. Soc.*, 142, 21767-21774, <https://doi.org/10.1021/jacs.0>
561 [c09683](https://doi.org/10.1021/jacs.0c09683), 2020.

562 Li, G., Bei, N., Cao, J., Huang, R., Wu, J., Feng, T., Wang, Y., Liu, S., Zhang, Q., Tie, X., and
563 Molina, L. T.: A possible pathway for rapid growth of sulfate during haze days in China,
564 *Atmos. Chem. Phys.*, 17, 3301-3316, <https://doi.org/10.5194/acp-17-3301-2017>, 2017.

565 Li, J., Zhang, Y. L., Cao, F., Zhang, W., Fan, M., Lee, X., and Michalski, G.: Stable sulfur
566 isotopes revealed a major role of transition-metal ion-catalyzed SO₂ oxidation in haze
567 episodes, *Environ. Sci. Technol.*, 54, 2626-2634, <https://doi.org/10.1021/acs.est.9b07150>,
568 2020.

569 Li, K., Kong, L., Zhankakova, A., Tong, S., Shen, J., Wang, T., Chen, L., Li, Q., Fu, H., and
570 Zhang, L.: Heterogeneous conversion of SO₂ on nano α -Fe₂O₃: the effects of morphology,
571 light illumination and relative humidity, *Environ. Sci.: Nano*, 6, 1838-1851,
572 <https://doi.org/10.1039/c9en00097f>, 2019.

573 Lim, S., Lee, M., Kim, S., and Laj, P.: Sulfate alters aerosol absorption properties in East Asian
574 outflow, *Sci. Rep.*, 8, 5172-5178, <https://doi.org/10.1038/s41598-018-23021-1>, 2018.

575 Liu, T., Clegg, S., and Abbatt, J. P. D.: Fast oxidation of sulfur dioxide by hydrogen peroxide
576 in deliquesced aerosol particles, *Proc. Natl. Acad. Sci. U. S. A.*, 117, 1354-1359,
577 <https://doi.org/10.1073/pnas.1916401117>, 2020a.

578 Liu, T., Chan, A. W. H., and Abbatt, J. P. D.: Multiphase oxidation of sulfur dioxide in aerosol
579 particles: Implications for sulfate formation in polluted environments, *Environ. Sci.*
580 *Technol.*, 55, 4227-4242, <https://doi.org/10.1021/acs.est.0c06496>, 2021.

581 Liu, Y., Deng, Y., Liu, J., Fang, X., Wang, T., Li, K., Gong, K., Bacha, A. U., Nabi, I., Ge, Q.,
582 Zhang, X., George, C., and Zhang, L.: A novel pathway of atmospheric sulfate formation
583 through carbonate radicals, *Atmos. Chem. Phys.*, 22, 9175-9197,
584 <https://doi.org/10.5194/acp-22-9175-2022>, 2022.

585 Ma, J., Dörner, S., Donner, S., Jin, J. L., Cheng, S. Y., Guo, J. R., Zhang, Z. F., Wang, J. Q.,
586 Liu, P., Zhang, G. Q., Pukite, J., Lampel, J., and Wagner, T.: MAX-DOAS measurements of
587 NO₂, SO₂, HCHO, and BrO at the Mt. Waliguan WMO GAW global baseline station in the
588 Tibetan Plateau, *Atmos. Chem. Phys.*, 20, 6973-6990, <https://doi.org/10.5194/acp-20-6973->
589 [2020](https://doi.org/10.5194/acp-20-6973-2020), 2020.

590 Ma, Q., Wang, L., Chu, B., Ma, J., and He, H.: Contrary role of H₂O and O₂ in the kinetics of
591 heterogeneous photochemical reactions of SO₂ on TiO₂, *J. Phys. Chem. A.*, 123, 1311-1318,
592 <https://doi.org/10.1021/acs.jpca.8b11433>, 2019.

593 Martins-Costa, M., Anglada, J., Francisco, J., and Ruiz-Lopez, M.: Photochemistry of SO₂ at
594 the air-water interface: A source of OH and HOSO radicals, *J. Am. Chem. Soc.*, 140, 12341-
595 12344, <https://doi.org/10.1021/jacs.8b07845>, 2018.

596 Mauldin, R., Berndt, T., Sipila, M., Paasonen, P., Petaja, T., Kim, S., Kurten, T., Stratmann, F.,
597 Kerminen, V., and Kulmala, M.: A new atmospherically relevant oxidant of sulphur dioxide,

598 Nature, 488, 193-196, <https://doi.org/10.1038/nature11278>, 2012.

599 Mukuta, T., Fukazawa, N., Murata, K., Inagaki, A., Akita, M., Tanaka, S., Koshihara, S. Y., and
600 Onda, K.: Infrared vibrational spectroscopy of $[\text{Ru}(\text{bpy})_2(\text{bpm})]^{2+}$ and $[\text{Ru}(\text{bpy})_3]^{2+}$ in the
601 excited triplet state, *Inorg. Chem.*, 53, 2481-2490, <https://doi.org/10.1021/ic402474t>, 2014.

602 Olson, E., Michalski, G., Welp, L., Valdivia, A., Larico, J., Pen, J., Fang, H., Gomez, K., and
603 Li, J.: Mineral dust and fossil fuel combustion dominate sources of aerosol sulfate in urban
604 Peru identified by sulfur stable isotopes and water-soluble ions, *Atmos. Environ.*, 260,
605 118482-118495, <https://doi.org/10.1016/j.atmosenv.2021.118482>, 2021.

606 Park, J. and Jang, M.: Heterogeneous photooxidation of sulfur dioxide in the presence of airborne
607 mineral dust particles, *RSC Adv.*, 6, 58617-58627, <https://doi.org/10.1039/c6ra09601h>,
608 2016.

609 Park, J., Jang, M., and Yu, Z.: Heterogeneous photo-oxidation of SO_2 in the presence of two
610 different mineral dust particles: Gobi and arizona dust, *Environ. Sci. Technol.*, 51, 9605-
611 9613, <https://doi.org/10.1021/acs.est.7b00588>, 2017.

612 Peng, Y., von Salzen, K., and Li, J.: Simulation of mineral dust aerosol with Piecewise Log-
613 normal Approximation (PLA) in CanAM4-PAM, *Atmos. Chem. Phys.*, 12, 6891-6914,
614 <https://doi.org/10.5194/acp-12-6891-2012>, 2012.

615 Prospero, J.: Long-range transport of mineral dust in the global atmosphere: Impact of African
616 dust on the environment of the southeastern United States, *Proc. Natl. Acad. Sci. U. S. A.*,
617 96, 3396-3403, <https://doi.org/10.1073/pnas.96.7.3396>, 1999.

618 Shao, J., Chen, Q., Wang, Y., Lu, X., He, P., Sun, Y., Shah, V., Martin, R. V., Philip, S., Song,
619 S., Zhao, Y., Xie, Z., Zhang, L., and Alexander, B.: Heterogeneous sulfate aerosol formation
620 mechanisms during wintertime Chinese haze events: air quality model assessment using
621 observations of sulfate oxygen isotopes in Beijing, *Atmos. Chem. Phys.*, 19, 6107-6123,
622 <https://doi.org/10.5194/acp-19-6107-2019>, 2019.

623 Shiraiwa, M., Ueda, K., Pozzer, A., Lammel, G., Kampf, C. J., Fushimi, A., Enami, S., Arangio,
624 A. M., Frohlich-Nowoisky, J., Fujitani, Y., Furuyama, A., Lakey, P. S. J., Lelieveld, J., Lucas,
625 K., Morino, Y., Poschl, U., Takahama, S., Takami, A., Tong, H., Weber, B., Yoshino, A., and
626 Sato, K.: Aerosol health effects from molecular to global scales, *Environ. Sci. Technol.*, 51,
627 13545-13567, <https://doi.org/10.1021/acs.est.7b04417>, 2017.

628 Sidebottom, H. W., Badcock, C. C., Jackson, G. E., Calvert, J. G., Reinhardt, G. W., and Damon,
629 E. K.: Photooxidation of sulfur dioxide, *Environ. Sci. Technol.*, 6, 72-79,
630 <https://doi.org/10.1080/00022470.1971.10469552>, 1972.

631 Solbrig, C. W. and Gidaspow, D.: Convective diffusion in a parallel plate duct with one catalytic
632 wall, laminar flow, first order reaction-part one, *Can. J. Chem. Eng.*, 45, 35-39,
633 [https://doi.org/10.1016/0304-5102\(89\)80197-X](https://doi.org/10.1016/0304-5102(89)80197-X), 1967.

634 Sumner, A. L., Menke, E. J., Dubowski, Y., Newberg, J. T., Penner, R. M., Hemminger, J. C.,
635 Wingen, L. M., Brauers, T. and Finlayson-Pitts, B. J. The nature of water on surfaces of
636 laboratory systems and implications for heterogeneous chemistry in the troposphere. *Phys.*
637 *Chem. Chem. Phys.*, 6, 604-613, <https://doi.org/10.1039/B308125G>, 2004.

638 Tohidi, R., Farahani, V., and Sioutas, C.: Real-time measurements of mineral dust concentration
639 in coarse particulate matter $\text{PM}_{10-2.5}$ by employing a novel optical-based technique in Los

640 Angeles, Sci. Total. Environ., 838, 156215-156226, <https://doi.org/10.1016/j.scitotenv.2022.156215>, 2022.

641

642 Urupina, D., Romanias, M. N., and Thevenet, F.: How relevant is it to use mineral proxies to
643 mimic the atmospheric reactivity of natural dust samples? A reactivity study using SO₂ as
644 probe molecule, Minerals, 11, 282-299, <https://doi.org/10.3390/min11030282>, 2021.

645 Urupina, D., Lasne, J., Romanias, M. N., Thiery, V., Dagsson-Waldhauserova, P., and Thevenet,
646 F.: Uptake and surface chemistry of SO₂ on natural volcanic dusts, Atmos. Environ., 217,
647 116942-116959, <https://doi.org/10.1016/j.atmosenv.2019.116942>, 2019.

648 Usher, C., Michel, A., and Grassian, V.: Reactions on mineral dust, Chem. Rev. , 103, 4883-
649 4939, <https://doi.org/10.1021/cr020657y>, 2003.

650 Usher, C., Al-Hosney, H., Carlos-Cuellar, S., and Grassian, V.: A laboratory study of the
651 heterogeneous uptake and oxidation of sulfur dioxide on mineral dust particles, J. Geophys.
652 Res-atmos. , 107, 4713-4729, <https://doi.org/10.1029/2002jd002051>, 2002.

653 Wang, J., Li, J., Ye, J., Zhao, J., Wu, Y., Hu, J., Liu, D., Nie, D., Shen, F., Huang, X., Huang,
654 D. D., Ji, D., Sun, X., Xu, W., Guo, J., Song, S., Qin, Y., Liu, P., Turner, J. R., Lee, H. C.,
655 Hwang, S., Liao, H., Martin, S. T., Zhang, Q., Chen, M., Sun, Y., Ge, X., and Jacob, D. J.:
656 Fast sulfate formation from oxidation of SO₂ by NO₂ and HONO observed in Beijing haze,
657 Nat. Commun., 11, 2844-2850, <https://doi.org/10.1038/s41467-020-16683-x>, 2020a.

658 Yao, M., Zhao, Y., Hu, M., Huang, D., Wang, Y., Yu, J. Z., and Yan, N.: Multiphase reactions
659 between secondary organic aerosol and sulfur dioxide: Kinetics and contributions to sulfate
660 formation and aerosol aging. Environ. Sci. Technol. Lett., 6, 768-774,
661 <https://doi.org/10.1021/acs.estlett.9b00657>, 2019.

662 Ye, J., Abbatt, J. P. D., Chan, A. W. H.: Novel pathway of SO₂ oxidation in the atmosphere:
663 Reactions with monoterpene ozonolysis intermediates and secondary organic aerosol.
664 Atmos. Chem. Phys., 18, 5549-5565, <https://doi.org/10.5194/acp-18-5549-2018>, 2018.

665 Wang, S., Zhou, S., Tao, Y., Tsui, W. G., Ye, J., Yu, J. Z., Murphy, J. G., McNeill, V. F., Abbatt,
666 J. P. D., and Chan, A. W. H.: Organic peroxides and sulfur dioxide in aerosol: Source of
667 particulate sulfate. Environ. Sci. Technol., 53, 10695-10704, <https://doi.org/10.1021/acs.est.9b02591>, 2019.

668

669 Wang, T., Liu, Y., Deng, Y., Fu, H., Zhang, L., and Chen, J.: The influence of temperature on
670 the heterogeneous uptake of SO₂ on hematite particles, Sci. Total. Environ., 644, 1493-1502,
671 <https://doi.org/10.1016/j.scitotenv.2018.07.046>, 2018.

672 Wang, T., Liu, Y. Y., Deng, Y., Cheng, H. Y., Yang, Y., Li, K. J., Fang, X. Z., and Zhang, L. W.:
673 Irradiation intensity dependent heterogeneous formation of sulfate and dissolution of ZnO
674 nanoparticles, Environ. Sci.: Nano, 7, 327-338, <https://doi.org/10.1039/c9en01148j>, 2020b.

675 Wang, Z., Wang, T., Fu, H., Zhang, L., Tang, M., George, C., Grassian, V. H., and Chen, J.:
676 Enhanced heterogeneous uptake of sulfur dioxide on mineral particles through modification
677 of iron speciation during simulated cloud processing, Atmos. Chem. Phys., 19, 12569-12585,
678 <https://doi.org/10.5194/acp-19-12569-2019>, 2019.

679 Yang, N., Tsona, N. T., Cheng, S., Li, S., Xu, L., Wang, Y., Wu, L., and Du, L.: Competitive
680 reactions of SO₂ and acetic acid on α -Al₂O₃ and CaCO₃ particles, Sci. Total. Environ., 699,
681 134362-134370, <https://doi.org/10.1016/j.scitotenv.2019.134362>, 2020.

682 Yang, W., Ma, Q., Liu, Y., Ma, J., Chu, B., and He, H.: The effect of water on the heterogeneous
683 reactions of SO₂ and NH₃ on the surfaces of α-Fe₂O₃ and γ-Al₂O₃, *Environ. Sci.: Nano*, 6,
684 2749-2758, <https://doi.org/10.1039/c9en00574a>, 2019.

685 Zhang, P., Chen, T., Ma, Q., Chu, B., Wang, Y., Mu, Y., Yu, Y., and He, H.: Diesel soot
686 photooxidation enhances the heterogeneous formation of H₂SO₄, *Nat. Commun.*, 13, 5364-
687 5372, <https://doi.org/10.1038/s41467-022-33120-3>, 2022.

688 Zhang, R., Gen, M., Huang, D., Li, Y., and Chan, C.: Enhanced sulfate production by nitrate
689 photolysis in the presence of halide ions in atmospheric particles, *Environ. Sci. Technol.*,
690 54, 3831-3839, <https://doi.org/10.1021/acs.est.9b06445>, 2020a.

691 Zhang, T., Yang, W., Han, C., Yang, H., and Xue, X.: Heterogeneous reaction of ozone with
692 syringic acid: Uptake of O₃ and changes in the composition and optical property of syringic
693 acid, *Environ. Pollut.*, 257, 113632-113638, <https://doi.org/10.1016/j.envpol.2019.113632>,
694 2020b.

695 Zhang, X., Zhuang, G., Chen, J., Wang, Y., Wang, X., An, Z., and Zhang, P.: Heterogeneous
696 reactions of sulfur dioxide on typical mineral particles, *J. Phys. Chem. B*, 110, 12588-12596,
697 <https://doi.org/10.1021/jp0617773>, 2006.

698 Zhang, Y., Bao, F., Li, M., Chen, C., and Zhao, J.: Nitrate-enhanced oxidation of SO₂ on mineral
699 dust: A vital role of a proton, *Environ. Sci. Technol.*, 53, 10139-10145,
700 <https://doi.org/10.1021/acs.est.9b01921>, 2019.

701 Zhang, Y., Bao, F., Li, M., Xia, H., Huang, D., Chen, C., and Zhao, J.: Photoinduced uptake
702 and oxidation of SO₂ on Beijing urban PM_{2.5}, *Environ. Sci. Technol.*, 54, 14868-14876,
703 <https://doi.org/10.1021/acs.est.0c01532>, 2020c.

704